

# Development of the Terrestrial Planet Finder Coronagraph Membrane V-Grooves

Gun-Shing Chen<sup>\*</sup>, Houfei Fang<sup>†</sup>, Timothy Y. Ho<sup>‡</sup>, Ubaldo Quijano<sup>§</sup>,  
William C Ledebor<sup>¶</sup>, Andrew Kissil<sup>#</sup>, Gregory Agnes<sup>\*\*</sup>  
*Jet Propulsion Laboratory  
California Institute of Technology  
4800 Oak Grove Drive  
Pasadena, California 91109-8099*

An innovative architecture of a V-groove membrane sunshield, which serves as both a thermal shield and a light baffle, has been developed for the Terrestrial Planet Finder Coronagraph. A preliminary design analysis has been conducted to determine the major design parameters and to verify the existence of the boom technologies. A packaging and deployment study has been accomplished. A thermal analysis has been carried out to verify the thermal performance of this architecture. A dynamic analysis of the membrane V-groove sunshield has also been performed to validate its dynamic characteristics. The feasibility of this architecture has been confirmed consequently.

## I. Introduction

The Terrestrial Planet Finder (TPF) mission will study all aspects of planets outside our solar system: from their formation and development in disks of dust and gas around newly forming stars to the presence and features of those planets orbiting the nearest stars; from the numbers at various sizes and places to their suitability as an abode for life<sup>1</sup>. The Terrestrial Planet Finder Coronagraph is a potential architecture under developing at Jet Propulsion Laboratory for this mission. Figures 1 to 2 show the TPF Coronagraph in both packaged and deployed configurations.

To control the coronagraph's thermal environment, the concept of a novel V-groove sunshield, which serves as both a thermal shield and as a light baffle, has been developed by this study. This paper will discuss the architecture, preliminary design analysis, packaging and deployment, thermal analysis, and the dynamic analysis of the membrane V-groove sunshield.

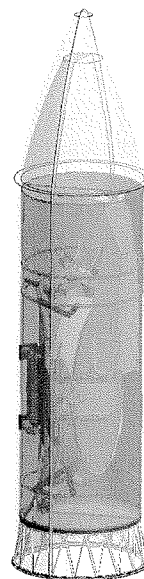


Figure 1. Stowed Configuration in Delta IV-H Fairing

<sup>\*</sup> Principal Engineer, Mechanical Systems Engineering and Research Division, Associate Fellow AIAA.

<sup>†</sup> Senior Engineer, Mechanical Systems Engineering and Research Division, Senior Member AIAA.

<sup>‡</sup> Member of Technical Staff, Mechanical Systems Engineering and Research Division.

<sup>§</sup> Academic Part Time Student

<sup>¶</sup> Member of Information Systems and Computer Science Staff, Observational Systems Division

<sup>#</sup> Senior Engineer, Mechanical Systems Engineering and Research Division, Senior Member AIAA

<sup>\*\*</sup> Senior Engineer, Mechanical Systems Engineering and Research Division, Senior Member AIAA

## II. Architecture of the membrane V-groove sunshield

With the development of materials and space gossamer technologies, large membrane sunshields are emerging and gaining more and more attentions<sup>2, 3</sup>. The sunshield developed by this study is a cocoon type V-groove membrane sunshield. It is composed of six layers of cone-shaped thin-membranes as shown in figure 3. The diameter of the most inner V-groove is 6.5 meters and the functional height of all V-grooves is 11.5 meters. The thickness of the membrane is 1-mil. Major components include: 1) membranes to serve as the sunshield, 2) catenary systems that stretch the membranes to give them stiffness, 3) booms which deploy the membranes and provide structural rigidity, 4) spacer bars to separate membranes, and 5) anchoring cables to stabilize the booms and to prevent bending loads to be loaded onto the booms. Figure 4 is the schematic of the cocoon type V-groove membrane sunshield.

Among these components, the deployable booms are the most critical structural components. They are of a great length (around 15 meters) and demanded to be lightweight. Every boom is requested to be packaged within a 0.3-meter diameter

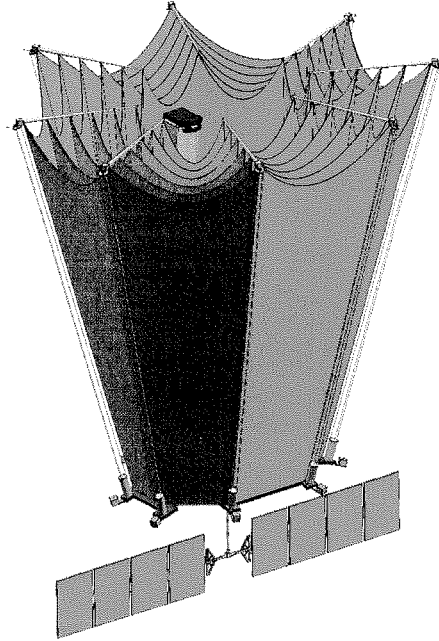


Figure 2. Deployed Configuration of Coronagraph, V-Groove Sunshield, and Solar Panel

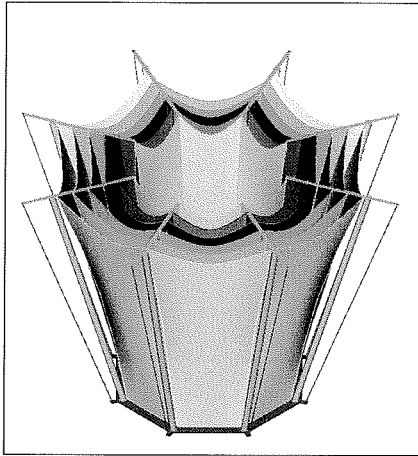


Figure 3. A V-Groove Sunshield System

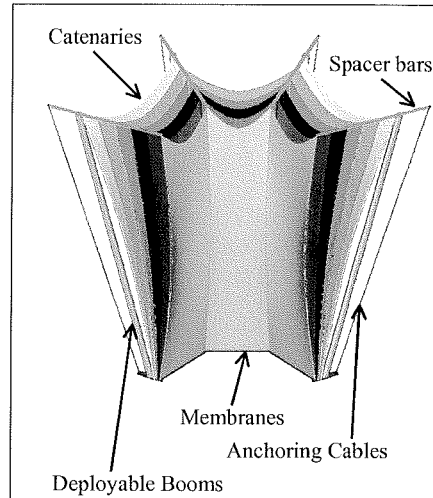


Figure 4. Schematic of the V-Groove Sunshield System

and 0.7-meter tall envelope to accommodate the system package as shown in figure 1. In order to minimize the bending moment on a boom introduced by the membrane tensioning force, an anchoring cable is employed by this architecture.

## III. Preliminary design analysis

After the architecture was developed, a preliminary design analysis was conducted to determine the parameters of the catenary systems, positions and orientations of booms, positions and orientations of anchoring cables, and forces loading the booms in their axial directions. The ultimate purpose of this analysis is to determine the feasibility of this architecture. Therefore, an extensive study of as many as 18 different boom technologies was conducted to

detect the existence of boom technologies that can accommodate this architecture. References 4 to 9 are some boom technologies that have been published in the public domain.

This study used 1-mil ( $2.54 \times 10^{-5}$  meter) thick aluminized Kapton as the membrane material. The membrane tensioning stress is assumed to be 3-psi ( $20689 \text{ N/m}^2$ ). Every V-groove is composed of 8 flat membrane sections. The bottom separation between two layers of membrane is given as 2 inches (5.08 cm) and the angle between two adjacent layers of membrane is 3 degrees. The most inner layer is a 6.5-meter diameter and 11.5-meter (excluding the catenary area) tall cylinder.

The preliminary design analysis started from the catenary analysis. A catenary is a cable that is connected to the edge of a piece of membrane. The function of the catenary is to evenly apply tensioning stress to a piece of membrane to stretch it. Figure 5 is an example of a piece of membrane that is tensioned by a catenary. Figure 6 is the curvature of a catenary. In figure 6,  $L$  is called the span of the catenary,  $h$  is called the sag of the catenary,  $w$  is the stress that the catenary applies to the membrane. After the span, sag, and membrane stress are determined, the force along the catenary cable can be calculated.<sup>10</sup> The cable forces of all six membrane are then used to calculate the force transmitted to a boom.

Figure 7 is a diagram that shows the locations and orientations of six layers of membranes, spacer bar, boom, and anchoring cable. After the catenary analyses, the magnitudes and directions of the forces acting on the spacer bar by catenaries are all determined. By applying force and moment balance with respect to the intersect point of the boom and the spacer bar, both boom force and anchoring cable force can be calculated correspondingly. Most lightweight boom technologies are developed to take large axial buckling loads with very limited bending capabilities. In order to minimize the bending load on a boom, the bending moment load on the boom is assumed to be zero

The variables of the preliminary design analysis are:

1. Sag of the catenary system. Since the orientations of different layers of membrane vary, it is required that the projections of all sags on the vertical axis must be at the same height. The dimension of the projections of all sags on the vertical axis is named as "sag of the catenary system".
2. Boom angle. The boom angle is defined as the angle between a boom and the vertical axis. The minimum boom angle is 16.18 deg, which is the angle of the outmost layer membrane.
3. Top offset. The top offset is defined as the distance between the center of the top end of the boom and the anchoring cable. Top offset is indicated as  $L$  in Figure 7. The minimum top offset is 0.15 meter.
4. Bottom offset. The bottom offset is defined as the distance between the center of the bottom end of the boom and the anchoring cable. The minimum bottom offset is 0.2 meter.
5. Boom force. The boom force is the force loaded on the boom in the axial direction of the boom.
6. Boom length. The boom length is the function of the sag of the catenary system as well as the angle of the boom.
7. Required boom bending stiffness. The assumptions made for analyzing bending stiffness are: the boom failure type is Euler buckle, bottom of the boom is fixed, top of the boom is free, and the safety factor is 4. The required boom bending stiffness is calculated as:



Figure 5. A piece of membrane that is tensioned

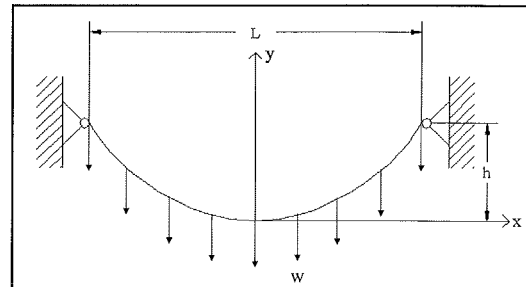


Figure 6. Curvature of a catenary

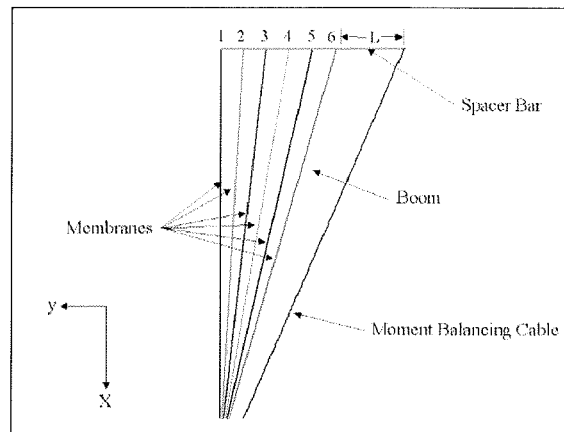
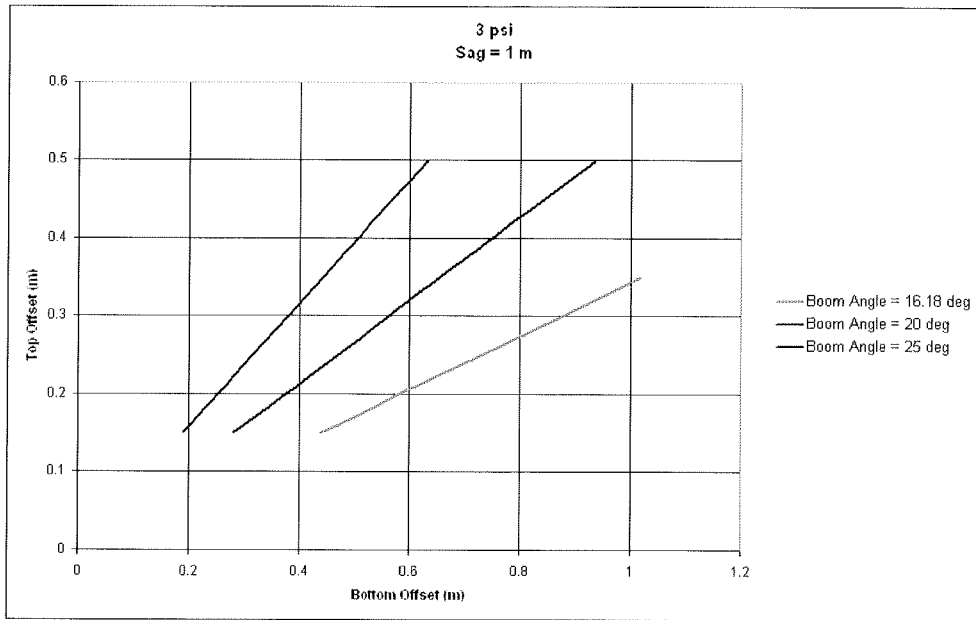


Figure 7. Orientations of the boom, membranes, spacer bar, and anchoring cable

$$EI = \alpha P \frac{(2L)^2}{\pi^2} \tag{1}$$

Where, L is the length of the boom, P is the applied boom force,  $\alpha$  is the safety factor.

Figures 8 to 11 are some of the preliminary design analysis results. Figure 8 shows the top offset as the function of the bottom offset while the sag of the catenary system is kept at 1 meter. Figure 9 shows the boom force as well as the required bending stiffness



**Figure 8. Top offset (sag equals to 1-meter)**

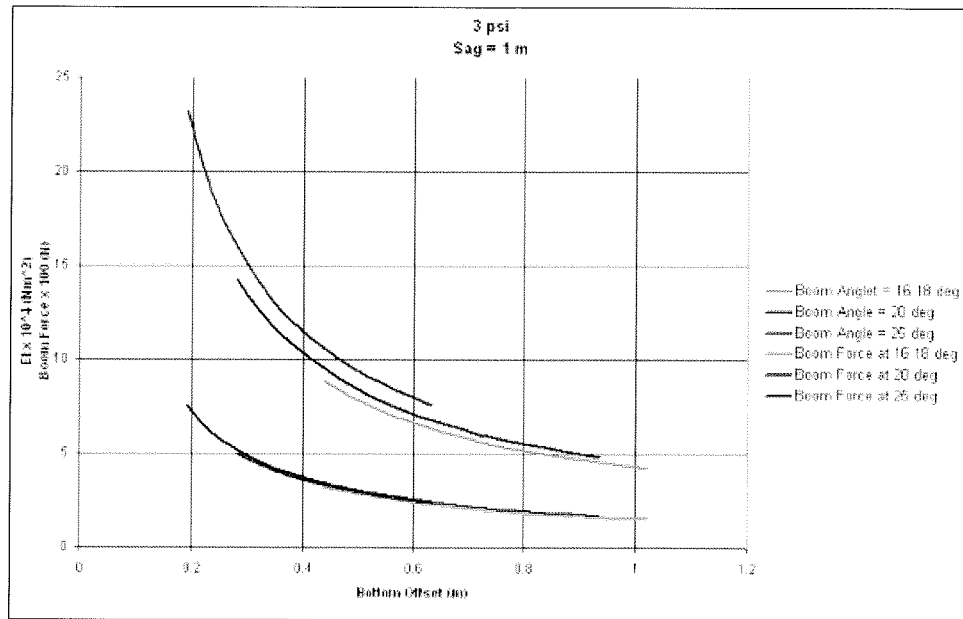


**Figure 9. Boom force as well as the required bending stiffness (sag equals to 1-meter)**

as the required bending stiffness (EI) as the function of the bottom offset while the sag of the catenary system is kept at 1 meter.

Figure 10 shows the top offset as the function of the bottom offset while the sag of the catenary system is kept at 2 meter. Figure 11 shows the boom force as well as the required bending stiffness (EI) as the function of the bottom offset while the sag of the catenary system is kept at 2 meter.

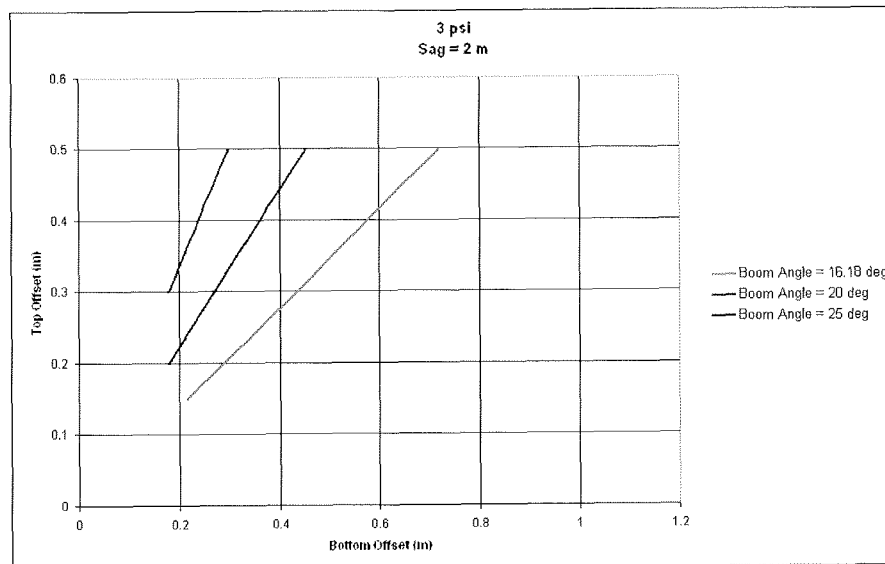


Figure 10. Top offset (sag equals to 2-meter)

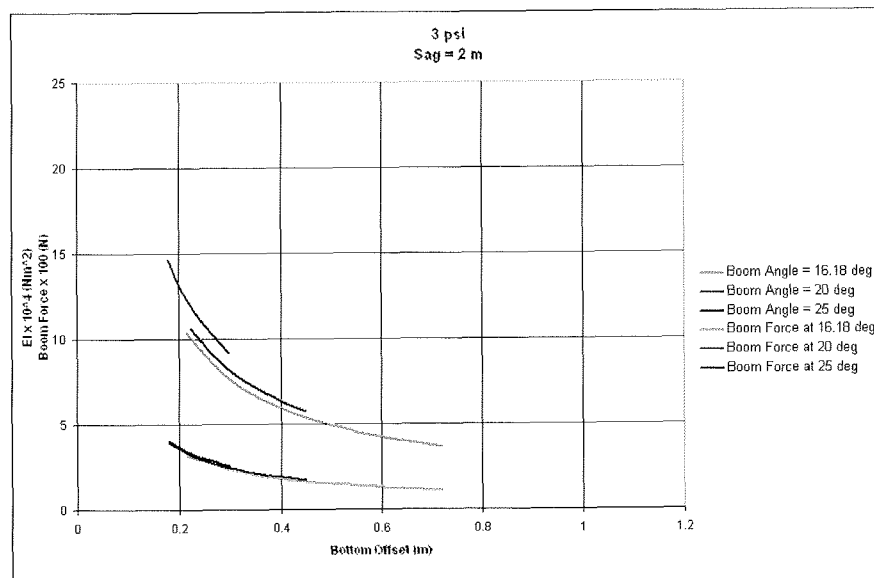


Figure 11. Boom force as well as the required bending stiffness (sag equals to 2-meter)

Following observations can be obtained from figures 8 to 11:

1. Smaller sag of the catenary system results in a bigger force that is loaded to the spacer bar by the catenary. The force loaded to the boom by the catenary via the spacer bar also becomes bigger. On the other hand, bigger sag requires longer boom. In order to minimize the required boom bending stiffness, shorter boom length and smaller boom force are preferred.
2. Smaller bottom offset is desired for packaging. Smaller bottom offset results in a smaller top offset and the system is more compact. However, smaller bottom offset is also associated with undesirable bigger boom force as well as bigger boom bending stiffness.
3. Bigger boom angle results to preferred smaller bottom offset as well as undesired boom force.

It is concluded by this analysis that there are existences of boom technologies that can be developed to accommodate this architecture. The potential boom technology, which can be further developed for this application, has also been identified consequently.

#### IV. Packaging and in-space deployment

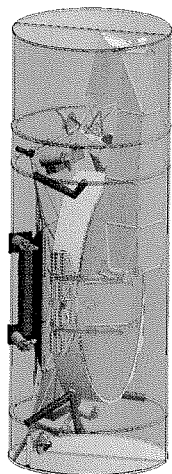


**Figure 12. Both coronagraph and sunshield are packaged in the fairing of a Delta IV-H**

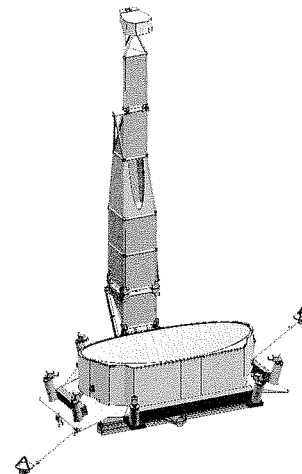


**Figure 13. Coronagraph is deployed while sunshield is still packaged**

One of the challenges of this study is to package the coronagraph and the membrane sunshield into a Delta IV-H fairing. Tremendous efforts have been made to accomplish this as well as to avoid any possible conflict between the coronagraph and the sunshield during the deployment process. Figure 12 shows both coronagraph and sunshield, which are packaged in the fairing of a Delta IV-H. The first step of the deployment process is the deployment of the coronagraph as shown in figure 13. The second step of the deployment process is the deployment of the sunshield as shown in figure 2.

Another challenge of this study is how to package a membrane cylinder as a whole piece without introducing too many creases after it is deployed. The deployment process of the membrane cylinder should not have any conflict with the deployed coronagraph. An origami technology was invented by this study and demonstrated in figures 14 to 16.



**Figure 14. A packaged paper cylinder**

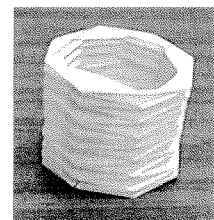


**Figure 15. A partially deployed paper cylinder**



**Figure 16. A fully deployed paper cylinder**

#### V. Thermal analysis of the V-groove sunshield

A thermal analysis was conducted to verify the thermal performance of the sunshield. Figures 17-18 give results of this analysis. It is concluded from the results of this analysis that this sunshield is capable to control the temperature environment of the coronagraph to meet the thermal requirements.

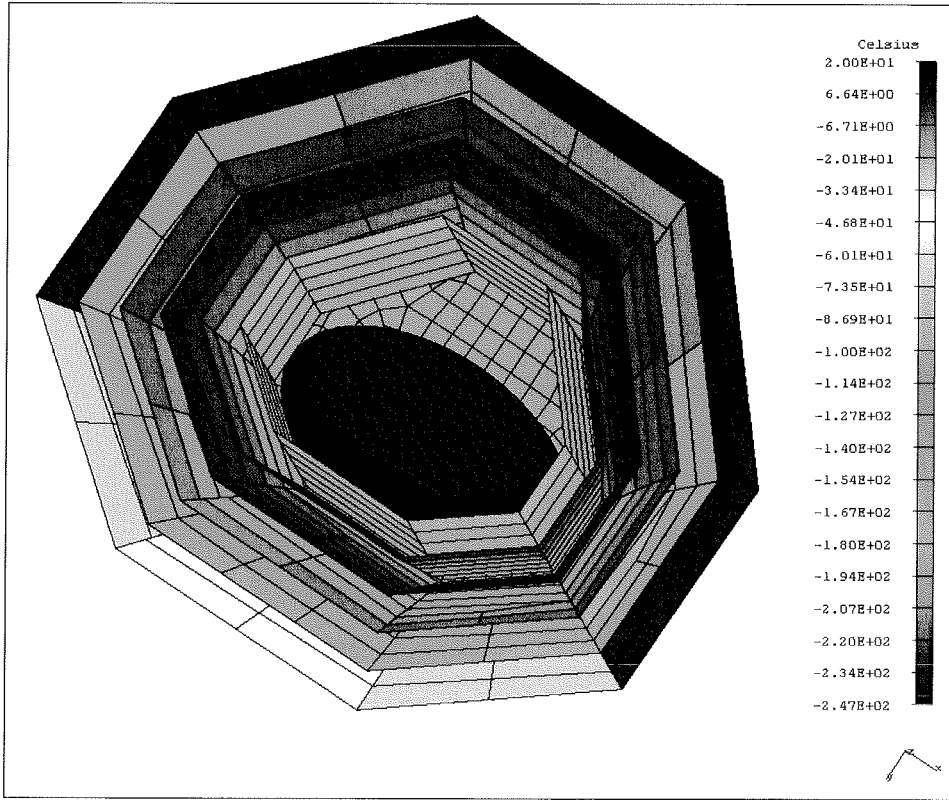


Figure 17. Temperature distribution with solar flux on +Y side of telescope

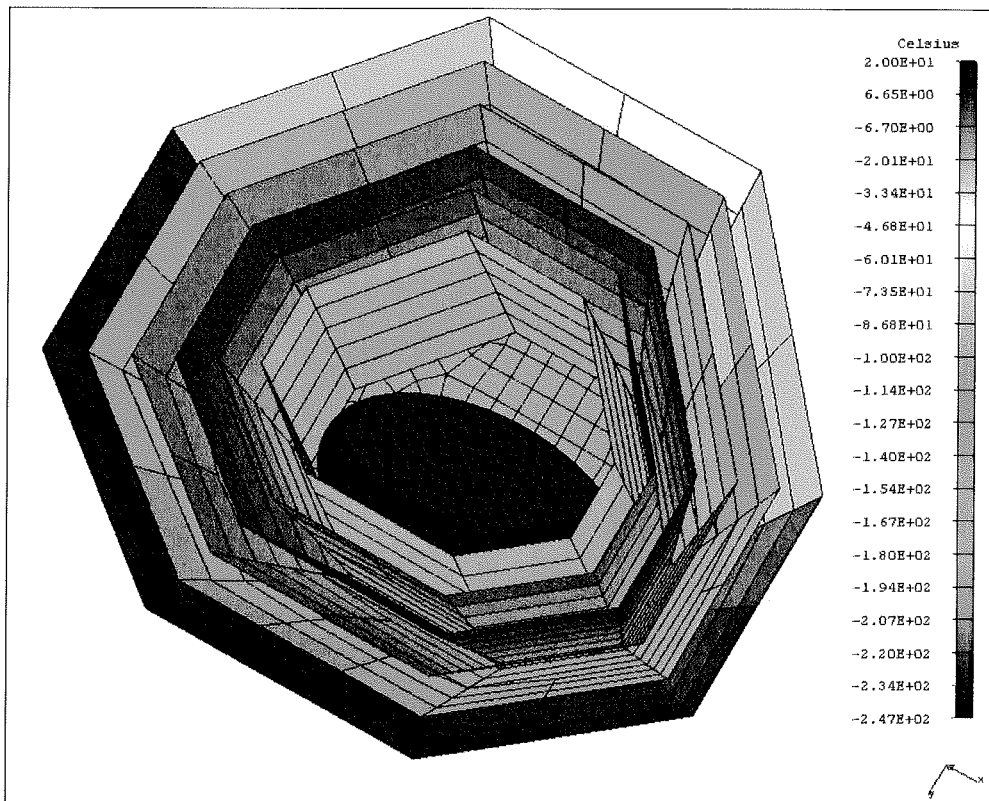
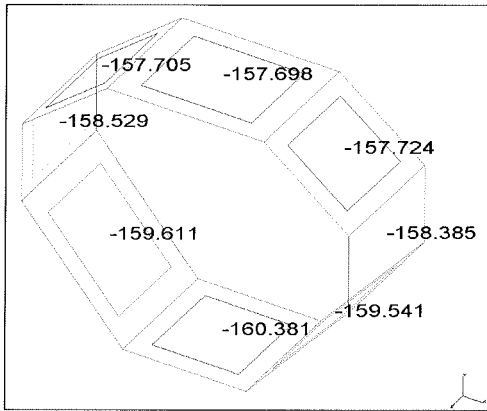


Figure 18. Temperature distribution with solar flux on -Y side of telescope

Two steady state cases were analyzed with the solar flux incident from opposite sides of the telescope. The difference in temperatures between these two cases gives a measure of how well the V-groove sunshield isolates the telescope from changes in the environment. As shown in Figures 19-20, the difference in temperature at the lower end of the inner shield (baffle) layer is  $\sim 0.5$  K. These steady state results represent a bounding case for a corresponding slew transient.

The two steady state temperature distributions were also used to calculate a wavefront error resulting from the distortion of the primary mirror.



**Figure 19. Temperature distribution on lower baffle with solar flux on +Y side of telescope**

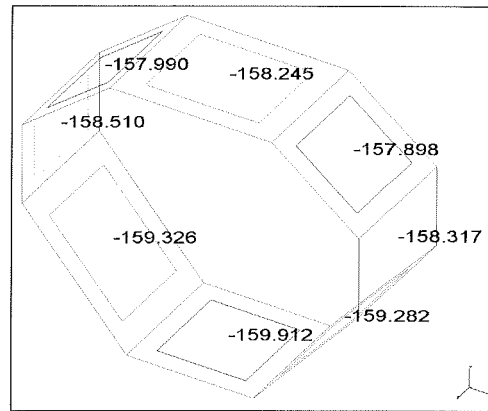


**Figure 20. Temperature distribution with solar flux on -Y side of telescope**

## VI. Dynamic analysis of the V-groove sunshield

A NASTRAN finite element model of the V-groove sunshield was created with the objective of capturing the first order effects of the system dynamics. In particular, it was important to adequately capture the low frequency modes which might influence the attitude control system, as well as modes which might couple with the dynamics of the critical optical

elements of the telescope. Although model accuracy is important, there is also a balancing factor of the need to minimize the model size. Smaller models are desirable from the standpoint of analysis turnaround time, which can be very significant when using Monte-Carlo approach to model parameter sensitivity studies.

Figure 21 shows a plot of the V-groove finite element model. The node density is rather coarse, but is just fine enough to capture the billowing modes of the flat portions of the sunshield.

The V-groove NASTRAN model was later translated into an IMOS (Integrated Modeling of Optical Systems) model, which uses the MATLAB environment for manipulating matrices. Minimizing model matrix size is an important factor in facilitating their manipulation in the MATLAB environment.

The approach chosen for modeling the pre-tensioned membranes incorporates a novel approximation of the geometric or load-stiffening effects, using the equivalent shear stiffness of standard plate elements. A similar approach can be used for modeling load-stiffened cables, or load-softened beams, using the standard beam element shear stiffness. Using the shear stiffness allows the sequence of modal frequencies to increase proportional to " $i$ " (mode number), rather than " $i^2$ " as one would get using the bending stiffness, the former being the case for load-stiffened cables and membranes as well. If one uses the bending stiffness to approximate the geometric stiffness, then only the first mode frequency can be matched: the higher modes would increase in frequency at a much higher rate, with respect to mode number, than would be the case associated with using the correct geometric stiffness.

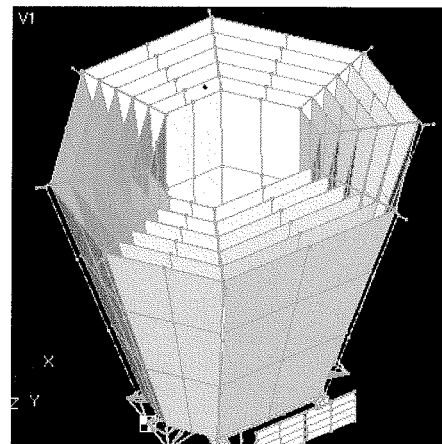


**Figure 21. FEM of V-groove Sunshield**

Another positive feature of using the standard element (beam or plate) shear stiffness to represent the geometric stiffness of load-stiffened structures is that there is no artificial grounding of the stiffness matrix, as one gets with many geometric stiffness formulations, such as encountered using NASTRAN's differential stiffness. Artificial grounding is especially critical for free-free systems, as we have with a space-borne telescope.

The modeling process for the load-stiffened members is simplified somewhat if one can make the assumption that bending stiffness is very minor compared the load-stiffening effects. If the stiffness is dominated by the load-stiffening effects, one can remove the bending stiffness from the problem by assigning an artificially high bending stiffness, such that the associated bending modes would occur at high enough frequencies that they are above the frequency range of interest. However, the bending stiffness should not be so high as to cause ill-conditioning problems.

If bending stiffness is an important factor, then a parallel set of nodes and elements can be defined on top of the elements used for modeling load-stiffening, and only the translational degrees of freedom would be connected between the two node sets.

One caveat in using this modeling approach is that one has to be careful in the attachment scheme used when connecting the load-stiffened members to non-load-stiffened members. Since the load-stiffened members have artificially high bending stiffness, they may introduce unrealistic constraints on adjacent bending-type elements. This potential problem can be avoided by using pin-flags, RBE2's or other mpc-type connections, where appropriate.

Another caveat is in the assumption of uniform preload stress. In reality, the preload stress may vary over the membrane, and may even go to zero in certain regions, allowing wrinkling and/or flapping. The modeling approach described herein doesn't account for such occurrences, but is mainly aimed at providing an early-on design aid, describing an ideal system. Once a feasible design is obtained, further detailed design and analysis should be pursued to address these issues, and how they might effect performance.

To model the load-stiffened membrane, the plate thickness and material properties are defined as usual. The bending factor should be set to a high value (again, not too high) to remove the bending flexibility from the model low frequency characteristics. The shear stiffness can then be tuned to match the correct geometric stiffness due to preload. The shear stiffness factor (TS/T in the PSHELL element property definition) should be set to the following:

$$\text{shear factor} = \text{Preload}/G, \tag{2}$$

where the Preload is the biaxial tension stress (i.e. lbs/in<sup>2</sup> or N/m<sup>2</sup>, etc), and G is the material shear modulus. For our V-groove model, we used 3psi (20703 N/m<sup>2</sup>) preload tension, and a G value of 190ksi (1.312e+9 N/m<sup>2</sup>) for the Kapton material. The in-plane membrane characteristics are not adversely effected by the above modeling definitions.

The minimum sunshield frequency was expected to occur at the outer (forward) edge of the widest flat segment (7.372m wide). The shape of this flat segment of the V-groove is approximately trapezoidal, with two equal length segments 12.5m long, a 7.372m long side, and a 4.4m long side. Two hand calculations were performed, using Ref 11, to estimate the expected first mode frequency: one with a fixed boundary rectangle 24m (twice the height of the trapezoid) by 7.372m, and one with a 12m by 7.372m rectangle having 2 free sides (opposite each other). The former case gives a frequency of 0.266Hz, and the latter case gives a lower bound frequency of 0.233Hz. Figure 22 shows a plot of the first mode of the sunshield finite element model, which was found to occur at 0.23Hz, which slightly underestimates compared to the hand calculations. The slight underestimation is due to the coarseness of the model.

A sunshield-only sub-model of the TPF system was analyzed to evaluate the effective mass characteristics. This model was constrained at the base of the deployable booms. Figure 23 shows a plot of the modal frequency as a function of mode number. We can see a very high modal density for the sunshield system: having approximately 200 modes less than 1Hz, and almost 1000 modes below 300 Hz.

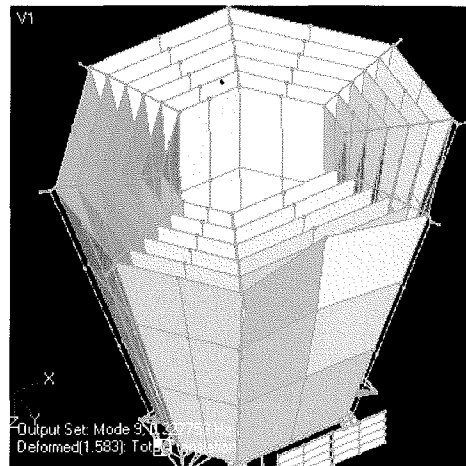


**Figure 22. First Mode of FEM V-groove Sunshield**

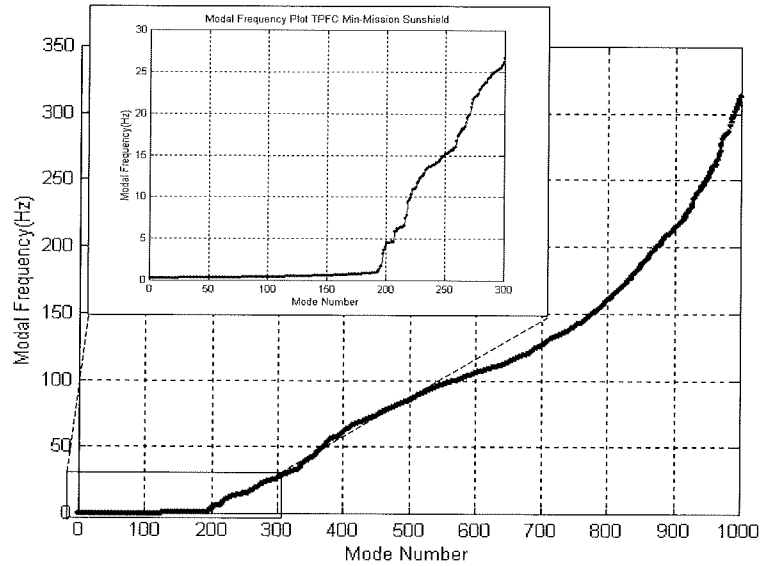


**Figure 23. Modal Frequencies for V-groove Sunshield**

Figure 24 shows a plot of the cumulative effective modal mass. There is a rather large jump in the translational effective masses in the xy plane at modes 198 and 199 (3.2 and 3.7Hz). The mode shape for mode 198 is shown in Figure 25. If one wants to capture 90% of the effective mass, then one would have to carry at least 500 modes to capture the translational terms, and at least 1000 modes to capture the rotational effective mass.

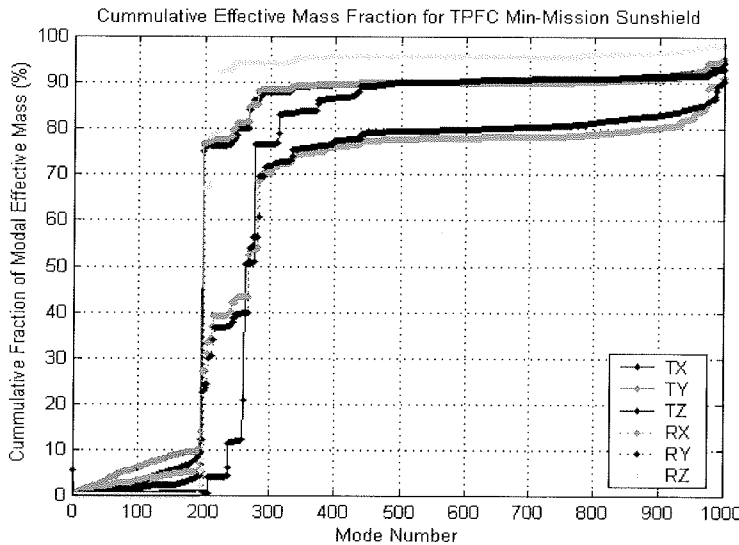


**Figure 24. Cumulative Effective Modal Mass for Cantilevered Sunshield**

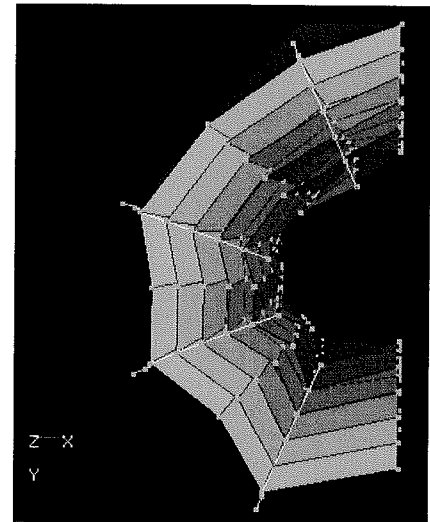


**Figure 25. Mode Shape for Mode 198 at 3.2Hz**

## VII. Concluding remarks

The architecture of a novel V-groove sunshield has been developed to control thermal environment of the Terrestrial Planet Finder Coronagraph. A preliminary design analysis has been conducted to determine the design parameters and to identify the boom technology. A packaging and deployment study has been accomplished. A thermal analysis has been carried out to verify the thermal performance of this architecture. A dynamic analysis of the membrane V-groove sunshield has also been performed to validate its dynamic characteristics. Followings are the conclusions made by this study:

1. There exist boom technologies that can accommodate this architecture.
2. It is doable to package the coronagraph and the membrane sunshield into a Delta IV-H fairing. Both coronagraph and sunshield can be deployed without any possible conflict between them during the deployment process.
3. The V-groove membrane sunshield is capable of controlling the temperature environment of the coronagraph to meet the thermal requirements.
4. The lowest frequency of the sunshield is calculated to be 0.25 Hz. Dynamic characteristics of the sunshield are satisfactory.

The ultimate conclusion is that the innovative architecture of the V-groove membrane sunshield developed by this study is feasible. Further development of this sunshield will be pursued.

### Acknowledgements

The work described in this paper was performed at the Jet Propulsion Laboratory, California Institute of Technology under contract with the National Aeronautics and Space Administration of United States.

### References

- <sup>1</sup>[http://planetquest.jpl.nasa.gov/TPF/tpf\\_index.html](http://planetquest.jpl.nasa.gov/TPF/tpf_index.html)
- <sup>2</sup>L. Pacini, and M. Lou, "Next Generation Space Telescope (NGST) Pathfinder experiment: Inflatable Sunshield In Space (ISIS)," October 1999, SAE 1999-01-5517
- <sup>3</sup>M. Mecham, "A Big Step Backward", Aviation /week & Space Technology, July 7, 2003
- <sup>4</sup>M. Lou, H. Fang, and L. Hsia, "Self- Rigidizable Space Inflatable Boom", AIAA Journal of Spacecraft and Rockets, Vol. 39, No.5, pp. 682-690, 2002
- <sup>5</sup>C. Hazelton, K. Gall, E. R. Abrahamson, R. J. Denis, M. Lake, "Development of a Prototype Elastic Memory Composite STEM for Large Space Structures", AIAA 2003-1977, 44<sup>th</sup> AIAA/ASME/ASCE/AHS/ASC Structures, Structural Dynamics, and Materials Conference and Exhibit, Norfolk, Virginia, April 2003
- <sup>6</sup>E. J. Simburger, et al., "Development, Design, and Testing of Powersphere Multifunctional Ultraviolet-Rigidizable Inflatable Structures", AIAA 2003-1897, 44<sup>th</sup> AIAA/ASME/ASCE/AHS/ASC Structures, Structural Dynamics, and Materials Conference and Exhibit, Norfolk, Virginia, April 2003
- <sup>7</sup>Charles R. Sandy, "Next Generation Space Telescope Inflatable Sunshield Development", IEEE 0-7803-5846-5, 2000
- <sup>8</sup><http://www.aec-able.com/Booms/ablebooms.html>
- <sup>9</sup>Koorosh Guidanean, David Lichodziejewski, "An Inflatable Rigidizable Truss Structure Based on New Sub-Tg Polyurethane Composites", AIAA 2002-1593, 43rd AIAA/ASME/ASCE/AHS/ASC Structures, Structural Dynamics, and Materials Conference, Denver, Colorado, 22-25 April 2002
- <sup>10</sup>H. Fang, M. Lou, L. Hsia, P. Leung, "Catenary Systems for Membrane Structures," AIAA 2001-1342, 42<sup>nd</sup> AIAA/ASME/ASCE/AHS/ASC Structures, Structural Dynamics, and Materials Conference and Exhibit, Seattle, WA, 16-19 April 2001
- <sup>11</sup>R.D. Blevins, Formulas for Natural Frequency and Mode Shape, 1979, Van Nostrand Reinhold Co. Inc., page 226